More than ADEQUATE: doubling the sensitivity of $^{13}C–^{13}C$ double-quantum NMR experiments

Justinas Sakas and Dušan Uhrín*

EaStCHEM School of Chemistry, University of Edinburgh, Edinburgh, UK.

E-mail: dusan.uhrin@ed.ac.uk

Electronic Supplementary Information

Table of Contents

Figures

Tables

1. Experimental parameters

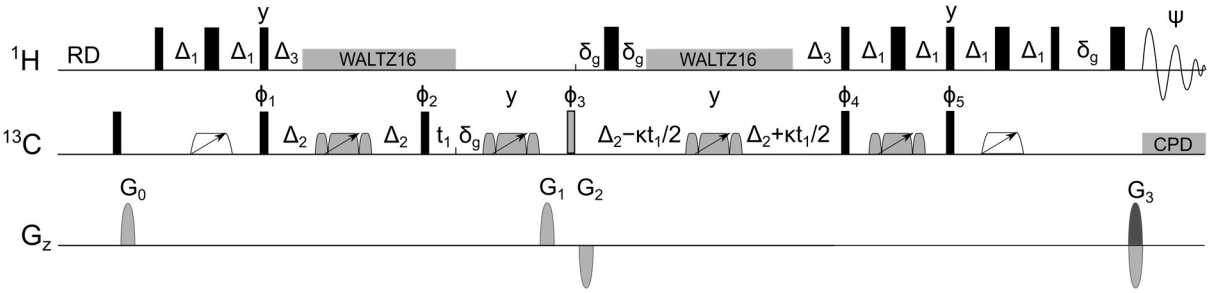

Fig. S1. $^1J_{CH}$-refocussed ADEQUATE pulse sequence. Narrow and wide bars represent 90° and 180° pulses, respectively. The grey narrow bar represents a 120° ^{13}C pulse. If κ = 0, double-quantum chemical shift is obtained in F_1. If κ = 1, single-quantum ^{13}C chemical shift is obtained in F_1. White and grey shapes with inclined arrows represent 180° inversion chirp (*Crp60,0.5,20.1*, 500 µs) and composite 180° refocussing chirp (*Crp60comp.4*, 2000 µs) pulses, respectively. Pulses were applied from the *x*-axis, unless stated otherwise; $\varphi_1 = x, -x$; $\varphi_2 = 4(y), 4(-y)$; $\varphi_3 = 8(y), 8(-y)$; $\varphi_4 = x, x, -x, -x$; $\varphi_5 = y, y, -y, -y$; $\psi = -y, y, y, -y, y, -y, -y, y, y, -y, -y, y, -y, y, y, -y$. The following delays were used: $\Delta_1 = 1/(4^1J_{CH})$, $\Delta_2 = 1/(4^{1,n}J_{CC})$, $\Delta_3 = 1/(2^1J_{CH})$, $\delta_g = 1.2$ ms. Smoothed square shaped gradient pulses of 1 ms duration were used, followed by a 0.2 ms recovery delay. The gradient strengths were: $G_0 = -23\%$, $G_1 = 78.5\%$, $G_2 = -77.6\%$, $G_3 = -59\%$, where 100% is equivalent to 53 G cm^{-1}. Phase-sensitive detection in F_1 was achieved by using echo-antiecho selection, by incrementing φ_5 by 180° and inverting the sign of G_3. GARP4 decoupling was used during acquisition.

The modified ADEQUATE experiments were developed based on *adeq11etgpsp* (DQ version) and *adeq11etgprdsp* (SQ version) pulse programs from the *TopSpin 4.1.4* library. The $^1J_{CH}$-refocussed ADEQUATE pulse sequences are shown in Fig. S1 and the Bruker pulse programs are provided in Sections 6 and 7 of the ESI. Spectra were recorded on a Bruker Avance Neo 800 MHz spectrometer equipped with a TCI three-channel cryoprobe using a 1.1 M sample of methyl β-D-xylopyranoside (**I**), a 32 mM sample of strychnine (**II**), and a 19.3 mM sample of fondaparinux (**III**). For **I** and **III**, Δ_1 and Δ_2 delays were optimised for $^1J_{CH} = 155$ Hz and $^1J_{CC} = 45$ Hz or $^nJ_{CC} = 6$ Hz, respectively; for **II**, they were optimised for $^1J_{CH} = 150$ Hz and $^1J_{CC} = 50$ Hz or $^nJ_{CC} = 6$ Hz, respectively. The spectra shown in Fig. S4 were recorded using a 0.5 M sample of L-isoleucine, optimised for $^1J_{CH} = 140$ Hz and $^1J_{CC} = 40$ Hz.

For $^1J_{CC}$-optimised ADEQUATE spectra of **I** and L-isoleucine, 1536 and 120 time domain points were acquired in F_2 and F_1, respectively. The ^{1}H and ^{13}C spectral widths were 6.07 and 70 ppm, corresponding to acquisition times of 158 ms and 4.3 ms in F_2 and F_1, respectively. The spectrometer offsets were set to 4.7 ppm and 78 ppm for ^{1}H and ^{13}C, respectively. 64 dummy scans, followed by 8 scans per increment were acquired for one-bond experiments. The relaxation delay was 1.5 s. The processed spectrum size was 4096×1024, with forward linear prediction in F_1 and zero filling in F_2; both dimensions were apodised using a cosine square window function. The total experiment time was 29 min 36 s.

For $^nJ_{CC}$-optimised ADEQUATE spectra of **I**, 1536 and 256 time domain points were acquired in F_2 and F_1, respectively. The ^{1}H and ^{13}C spectral widths were 6.07 and 70 ppm, corresponding to acquisition times of 158 ms and 9.1 ms in F_2 and F_1, respectively. The spectrometer offsets were set to 4.7 ppm and 78 ppm for ^{1}H and ^{13}C, respectively. 64 dummy scans, followed by 16 scans per increment were acquired for one-bond experiments. The relaxation delay was 1.5 s. The processed spectrum size was 4096×1024, with forward linear prediction in F_1 and zero filling in F_2; both dimensions were apodised using a cosine square window function. The total experiment time was 2 h 10 min.

For $^{1}J_{CC}$-optimised ADEQUATE spectra of **II**, 1536 and 192 time domain points were acquired in F_2 and F_1, respectively. The ^{1}H and ^{13}C spectral widths were 7.82 and 160 ppm, corresponding to acquisition times of 123 ms and 3.0 ms in F_2 and F_1, respectively. The spectrometer offsets were set to 4.7 ppm and 100 ppm for ^{1}H and ^{13}C, respectively. 80 scans per increment were acquired, with a relaxation delay of 1.5 s and 128 dummy scans. The processed spectrum size was 4096×1024, with forward linear prediction in F_1 and zero filling in F_2; both dimensions were apodised using a cosine square window function. The total experiment time was 7 h 18 min.

For $^{n}J_{CC}$-optimised ADEQUATE spectra of **II**, 1536 and 192 time domain points were acquired in F_2 and F_1, respectively. The ^{1}H and ^{13}C spectral widths were 7.82 and 160 ppm, corresponding to acquisition times of 123 ms and 3.0 ms in F_2 and F_1, respectively. The spectrometer offsets were set to 4.7 ppm and 100 ppm for ^{1}H and ^{13}C, respectively. 160 scans per increment were acquired, with a relaxation delay of 1.5 s and 128 dummy scans. The processed spectrum size was 4096×1024, with forward linear prediction in F_1 and zero filling in F_2; both dimensions were apodised using a cosine square window function. The total experiment time was 15 h 47 min.

For $^{1}J_{CC}$-optimised ADEQUATE spectra of **III**, 1536 and 118 time domain points were acquired in F_2 and F_1, respectively. The ^{1}H and ^{13}C spectral widths were 6.07 and 70 ppm, corresponding to acquisition times of 158 ms and 4.2 ms in F_2 and F_1, respectively. The spectrometer offsets were set to 4.7 ppm and 78 ppm for ^{1}H and ^{13}C, respectively. 128 scans per increment were acquired, with a relaxation delay of 1.5 s and 128 dummy scans. The processed spectrum size was 4096×1024, with forward linear prediction in F_1 and zero filling in F_2; both dimensions were apodised using a cosine square window function. The total experiment time was 7 h 20 min.

For $^{n}J_{CC}$-optimised ADEQUATE spectra of **III**, 1536 and 160 time domain points were acquired in F_2 and F_1, respectively. The ^{1}H and ^{13}C spectral widths were 6.07 and 70 ppm, corresponding to acquisition times of 158 ms and 5.7 ms in F_2 and F_1, respectively. The spectrometer offsets were set to 4.7 ppm and 78 ppm for ^{1}H and ^{13}C, respectively. 256 scans per increment were acquired, with a relaxation delay of 1.5 s and 64 dummy scans. The processed spectrum size was 4096×1024, with forward linear prediction in F_1 and zero filling in F_2; both dimensions were apodised using a cosine square window function. The total experiment time was 21 h 26 min.

2. Removal of cancellation artefacts

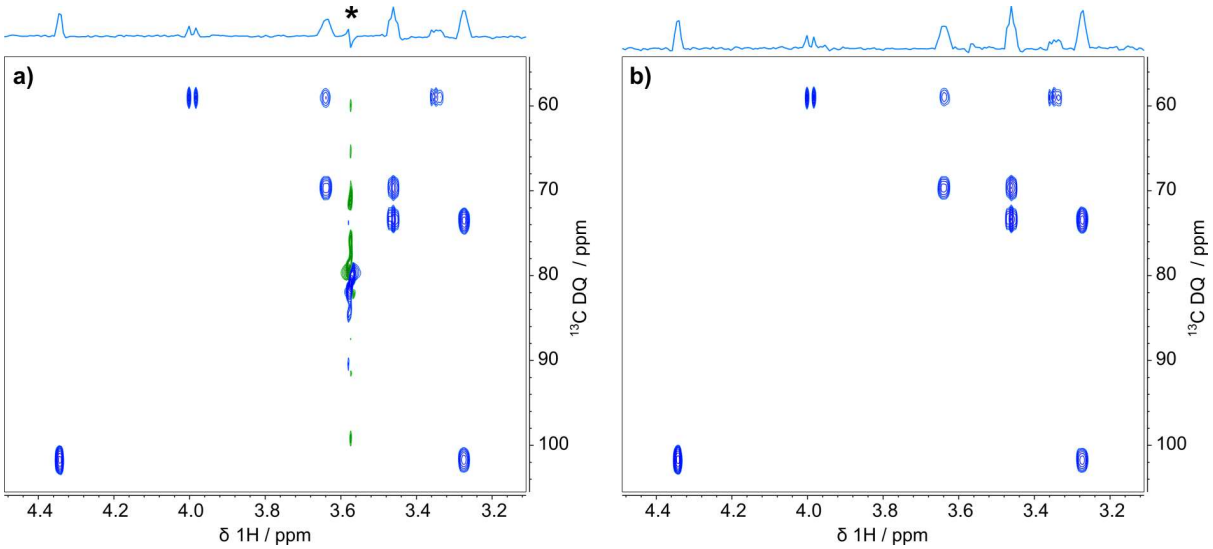

Fig. S2. Removal of cancellation artefacts using a purge element. 800 MHz $^{1}J_{CC}$-optimised DQ ADEQUATE spectrum of **I** recorded using the (a) Bruker library ADEQUATE pulse sequence *adeq11etgpsp* and (b) with the addition of the 90°-gradient purge element, which significantly reduced the CH_3 cancellation artefacts (*). Both spectra were recorded using identical parameters.

3. Comparison of ADEQUATE spectra of methyl β-D-xylopyranoside, I

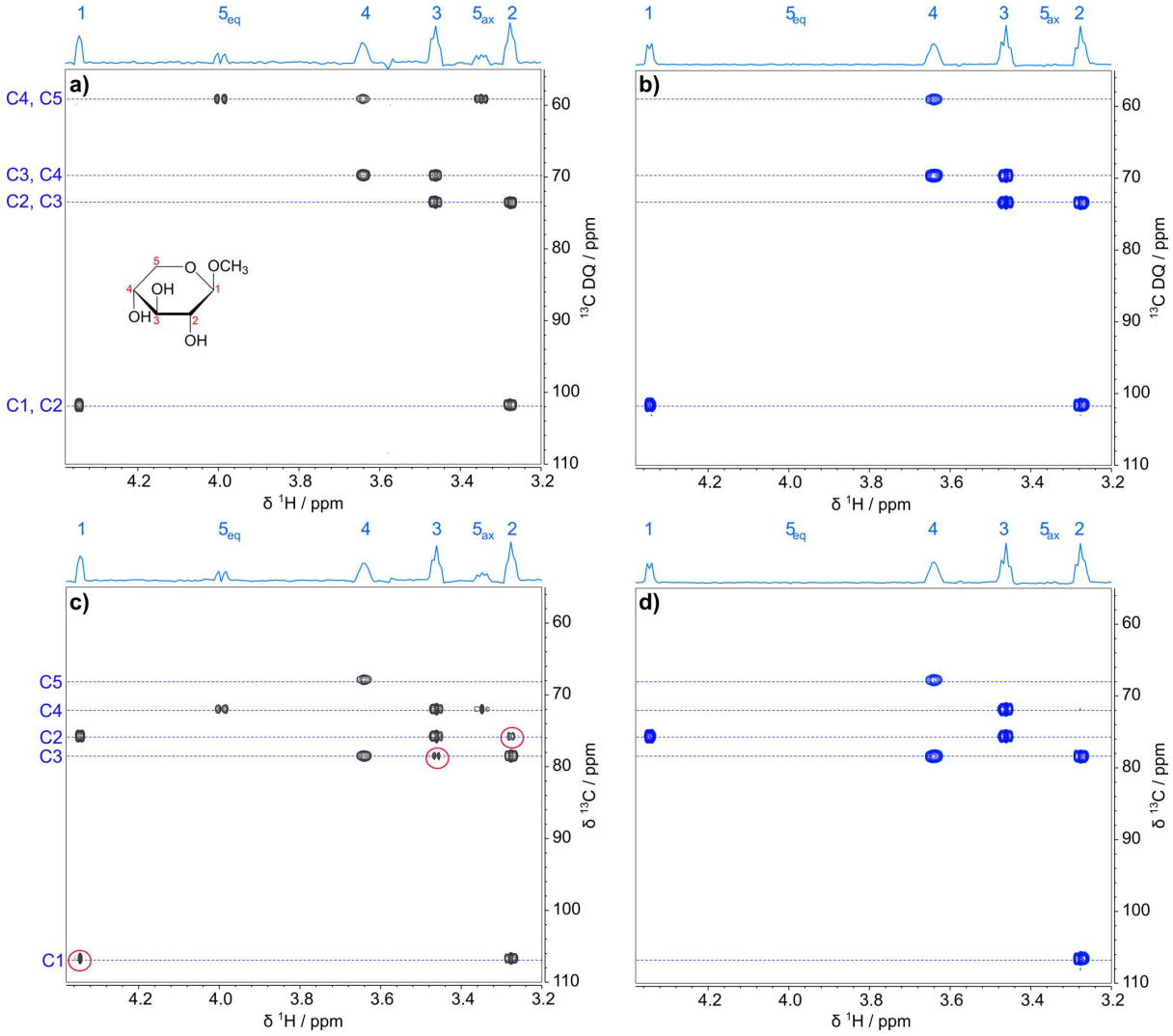

Fig. S3. Comparison of $^{1}J_{CC}$-optimised ADEQUATE spectra of **I**. (a) DQ ADEQUATE without $^{1}J_{CH}$ refocussing, (b) DQ ADEQUATE with $^{1}J_{CH}$ refocussing, (c) SQ ADEQUATE without $^{1}J_{CH}$ refocussing, and (d) SQ ADEQUATE with $^{1}J_{CH}$ refocussing. The DQ ADEQUATE spectra report DQ ^{13}C frequency and coupled ^{13}C nuclei appear at the same chemical shift, whereas the SQ ADEQUATE spectra report the conventional ^{13}C SQ chemical shifts at ^{1}H frequencies of the coupled carbons. The addition of $^{1}J_{CH}$ refocussing increases the intensity of CH-detected correlations only, therefore the H5 signals are missing/weak in the refocussed spectra. Note that the HSQC-like artefacts (circled in red), which appear in the standard SQ ADEQUATE spectrum, are removed by using $^{1}J_{CH}$ refocussing. All 2D spectra were plotted at the same intensity level. Positive projections plotted to scale are presented in Fig. 2 in the main text.

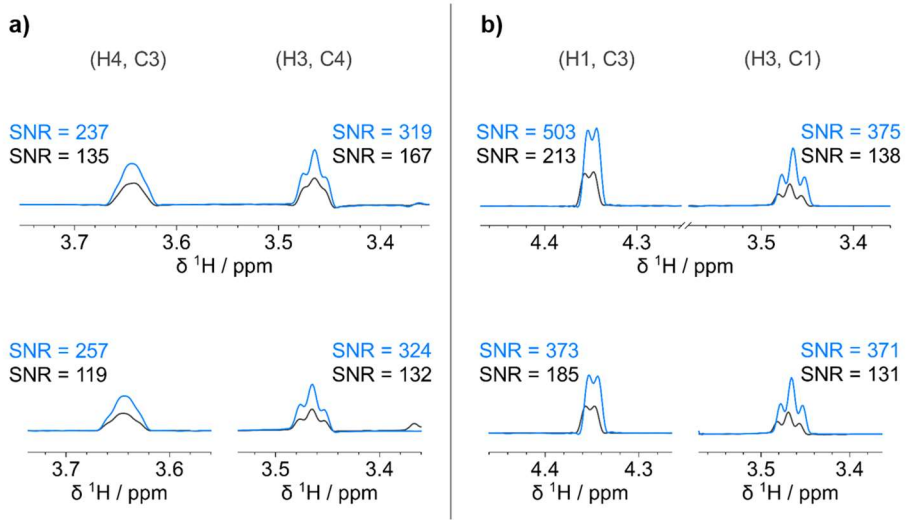

Fig. S4. SNR improvement for **I** in the $^{1}J_{CH}$-refocussed ADEQUATE experiments (blue traces) optimised for (a) $^{1}J_{CC}$ = 45 Hz and (b) $^{n}J_{CC}$ = 6 Hz. The top spectra, obtained using the DQ ADEQUATE, show the correlated spins sharing a ^{13}C DQ frequency, whereas for the bottom traces, obtained using SQ ADEQUATE, the corresponding correlations appear at different ^{13}C frequencies.

4. CH-detected CH_2, CH_3 and C_q correlations of L-isoleucine

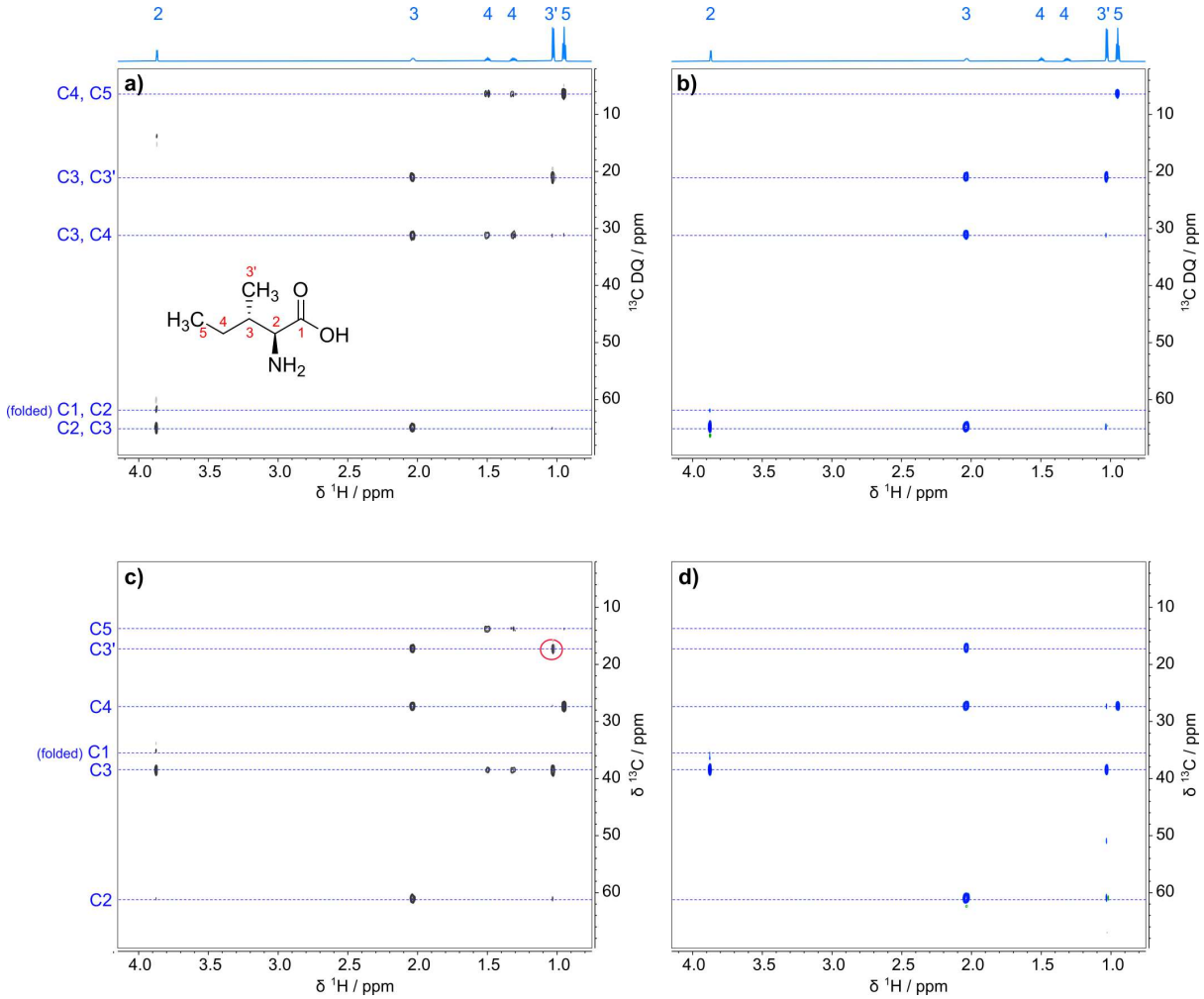

Fig. S5. Comparison of $^1J_{CC}$-optimised ADEQUATE spectra of L-isoleucine: (a) DQ ADEQUATE without $^1J_{CH}$ refocussing, (b) DQ ADEQUATE with $^1J_{CH}$ refocussing, (c) SQ ADEQUATE without $^1J_{CH}$ refocussing, and (d) SQ ADEQUATE with $^1J_{CH}$ refocussing. The spectra were acquired using the same parameters as described for **I**. All spectra are plotted at the same intensity level. Although the $^1J_{CH}$ refocussing decreases the sensitivity of CH_3-detected (and more substantially the CH_2-detected) coherences, connectivity information is not lost as the sensitivity of CH-detected CH–CH_2, CH–CH_3 and CH–C_q coherences is improved 1.3–2.0×. An HSQC-like artefact seen in (c) is circled in red. 1D ^{1}H NMR spectra of L-isoleucine are shown at the top.

5. Comparison of ADEQUATE spectra of strychnine, II

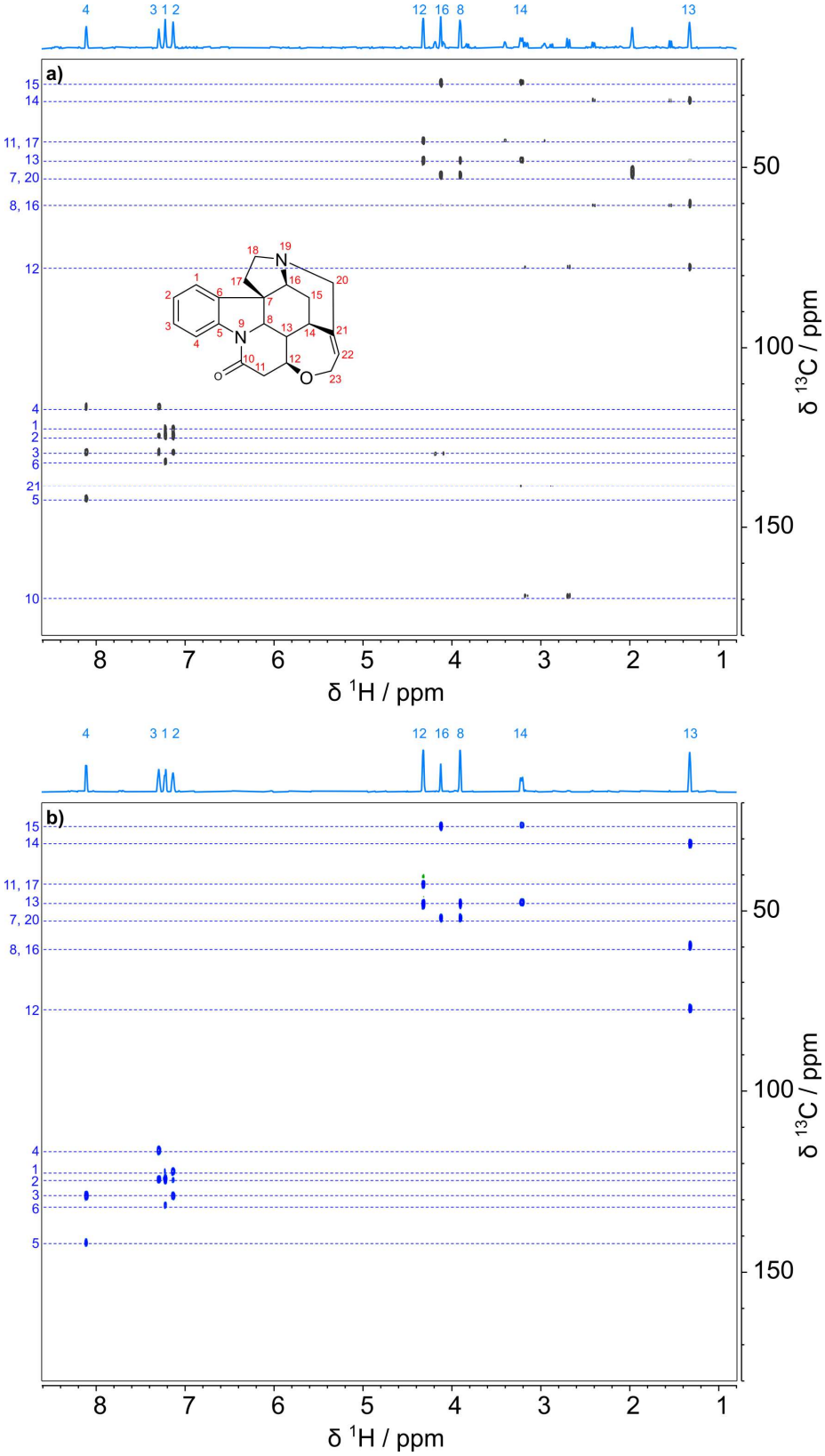

Fig. S6. $^{1}J_{CC}$-optimised SQ ADEQUATE spectra of **II** (a) without $^{1}J_{CH}$ refocussing, (b) with $^{1}J_{CH}$ refocussing. The spectra were plotted at the same intensity level. For detailed SNR comparison, see Table S1.

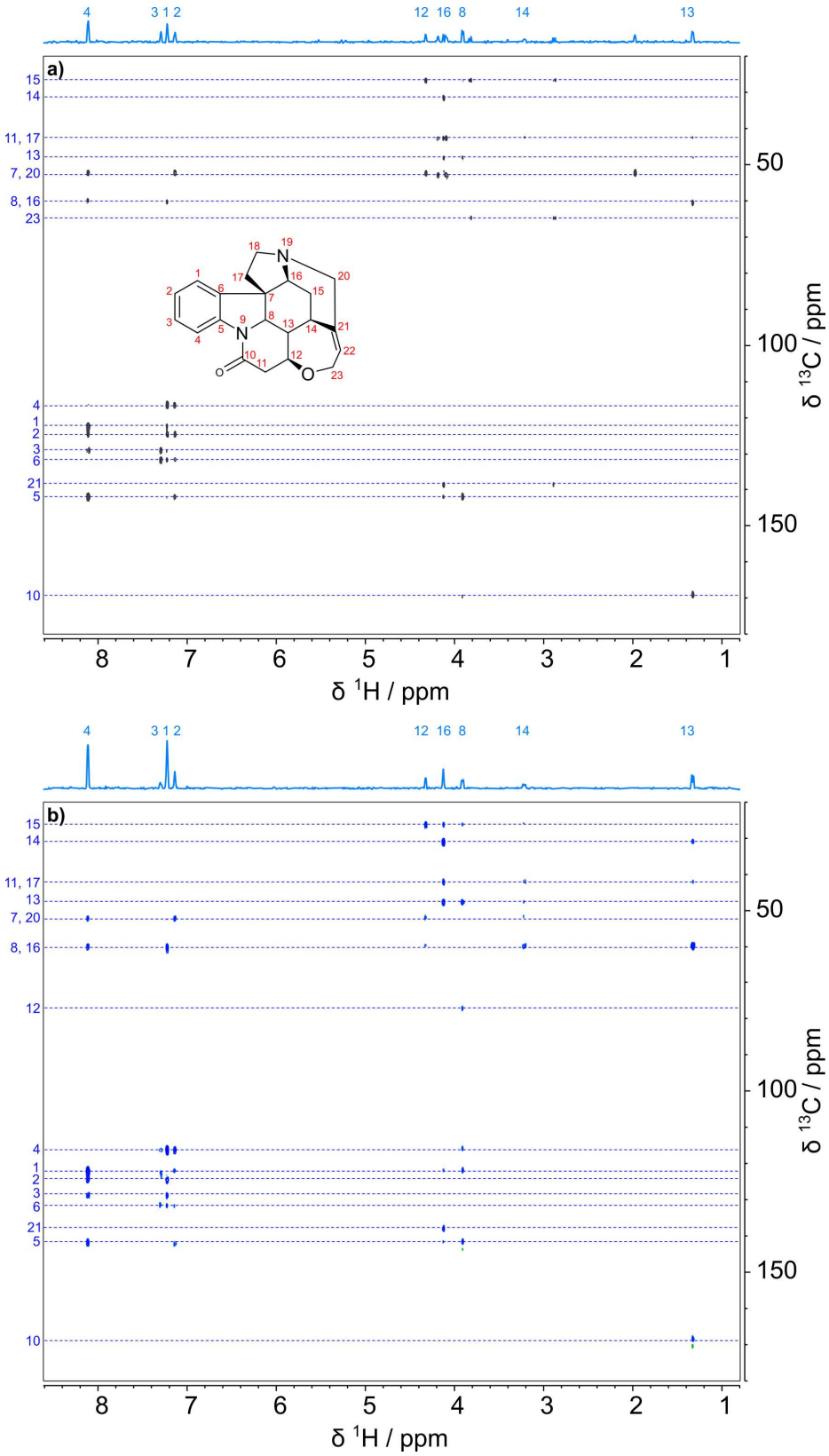

Fig. S7. $^{n}J_{CC}$-optimised SQ ADEQUATE spectra of **II** (a) without $^{1}J_{CH}$ refocussing, (b) with $^{1}J_{CH}$ refocussing. The spectra were plotted at the same intensity level. For detailed SNR comparison, see Table S2.

Table S1. Signal-to-noise ratio (SNR) comparison for CH-detected correlations of **II** observed in $^{1}J_{CC}$-optimised SQ ADEQUATE spectra with and without $^{1}J_{CH}$ refocussing.

Correlation (^{1}H, ^{13}C)	Signal-to-noise ratio		**Correlation (^{1}H, ^{13}C)**	Signal-to-noise ratio	
	standard	$^{1}J_{CH}$-refocussed		standard	$^{1}J_{CH}$-refocussed
1, 2[a]	14.5	31.8	12, 11[b]	26.6	32.3
1, 6[c]	21.8	17.6	12, 13[a]	31.6	45.1
2, 1[a]	11.9	20.3	13, 8[a]	22.1	50.6
2, 3[a]	14.8	26.8	13, 12[a]	17.0	49.9
3, 2[a]	13.0	26.7	13, 14[a]	21.1	47.5
3, 4[a]	14.2	29.2	14, 13[a]	12.4	16.2
4, 3[a]	22.7	36.1	14, 15[b]	12.2	12.9
4, 5[c]	18.7	17.7	16, 7[c]	35.4	31.7
8, 7[c]	28.6	25.9	16, 15[b]	30.0	34.8
8, 13[a]	29.8	44.9			

[a] CH–CH, [b] CH–CH_2, [c] CH–C_q correlations.

Table S2. Signal-to-noise ratio (SNR) comparison for CH-detected correlations of **III** observed in $^{n}J_{CC}$-optimised SQ ADEQUATE spectra with and without $^{1}J_{CH}$ refocussing.

Correlation (^{1}H, ^{13}C)	Signal-to-noise ratio		**Correlation (^{1}H, ^{13}C)**	Signal-to-noise ratio	
	standard	$^{1}J_{CH}$-refocussed		standard	$^{1}J_{CH}$-refocussed
1, 3[a]	3.7	7.7	8, 4[a]	– [e]	5.4
1, 4[a]	15.7	45.2	8, 5[c]	11.8	8.6
1, 5[c]	3.8	2.7[d]	12, 15[b]	7.0	9.2
1, 7[c]	3.6	5.3	12, 7[c]	6.7	7.0
1, 8[a]	5.5	13.8	12, 8[a]	3.0[d]	4.1
2, 4[a]	7.7	17.5	13, 10[c]	5.1	7.0
2, 5[c]	6.3	5.1	13, 11[b]	3.1	5.2
2, 6[c]	4.4	4.3	13, 16[a]	4.3	12.1
2, 7[c]	8.0	9.4	13, 7[c]	2.2[d]	4.0
3, 1[a]	2.0[d]	4.6	14, 11[b]	3.9	5.1
3, 5[c]	2.5[d]	3.3	14, 7[c]	4.1	3.7
3, 6[c]	7.6	6.5	14, 8[a]	2.8[d]	5.3
4, 1[a]	15.9	41.2	16, 1[a]	– [e]	5.0
4, 2[a]	7.7	11.8	16, 13[a]	4.1	15.1
4, 7[c]	9.7	8.2	16, 14[a]	6.1	16.8
4, 8[a]	4.9	9.4	16, 17[b]	3.5	8.7
8, 1[a]	4.1	8.3	16, 21[c]	5.9	8.4
8, 12[a]	– [e]	5.3	16, 5[c]	5.7	5.2
8, 15[b]	5.1	4.8			

[a] CH–CH, [b] CH–CH_2, [c] CH–C_q correlations. [d] Correlations with SNR ≤ 3 cannot be distinguished from noise without prior knowledge. [e] Not observed.

6. Comparison of ADEQUATE spectra of fondaparinux, III

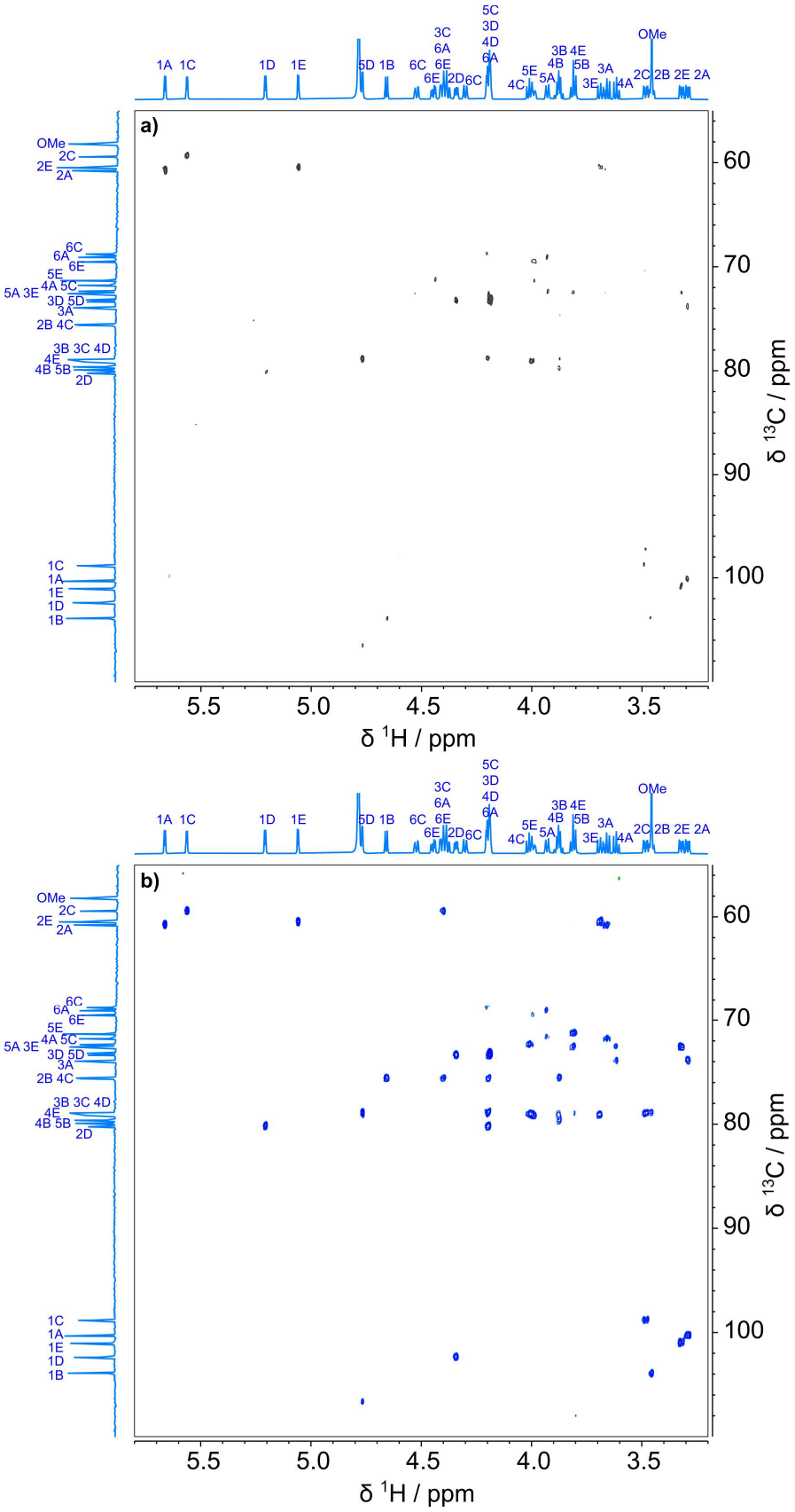

Fig. S8. $^{1}J_{CC}$-optimised SQ ADEQUATE spectra of **III** (a) without $^{1}J_{CH}$ refocussing, (b) with $^{1}J_{CH}$ refocussing. The spectra were plotted at the same intensity level.

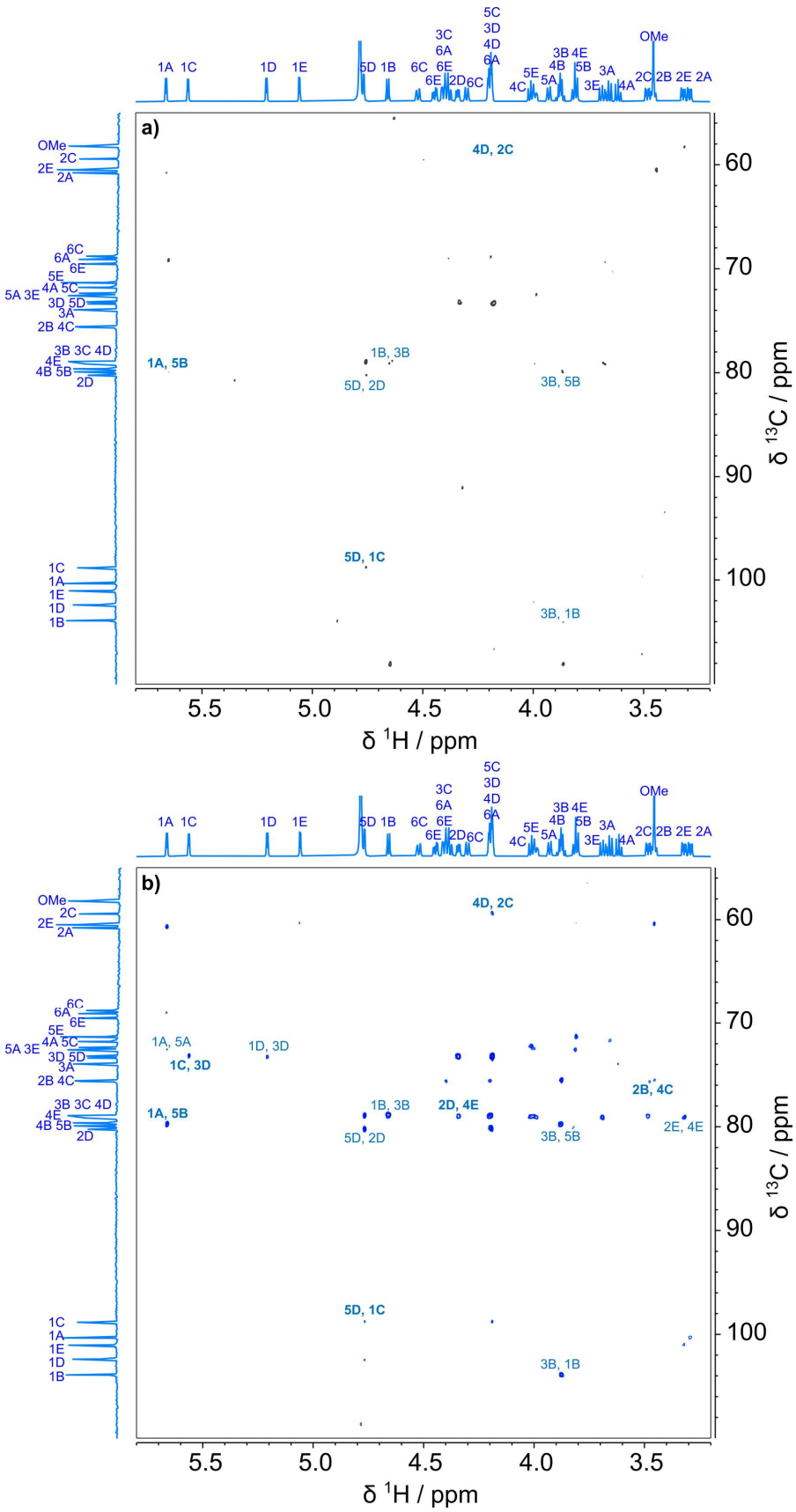

Fig. S9. $^{n}J_{CC}$-optimised SQ ADEQUATE spectra of **III** (a) without $^{1}J_{CH}$ refocussing, (b) with $^{1}J_{CH}$ refocussing. Correlations across glycosidic linkages are labelled in bold. Spectra were plotted at the same intensity level. The unlabelled cross peaks are due to one-bond C–C correlations (*cf.* Fig. S8).

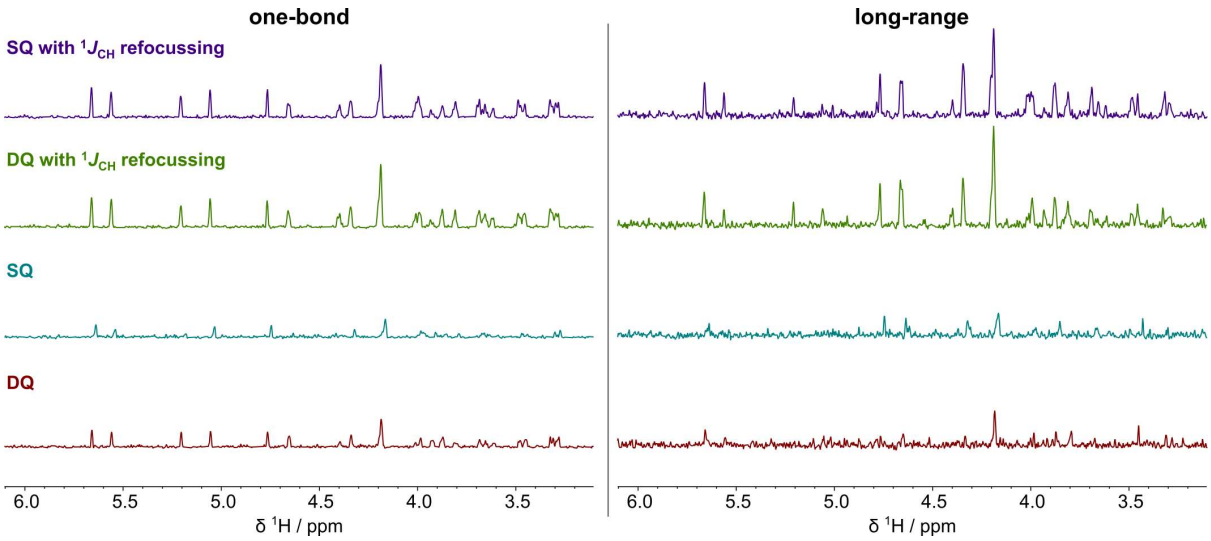

Fig. S10. Projections of ADEQUATE spectra of **III** optimised for one-bond (45 Hz, 128 scans) and long-range (6 Hz, 256 scans) J_{CC} couplings. Projections in the same column are plotted to scale.

The comparisons of SQ ADEQUATE spectra with and without $^1J_{CH}$ refocussing are shown in **Fig. S8** and **Fig. S9** for one-bond and long-range–optimised correlations, respectively. To-scale positive projections, including DQ ADEQUATE (full 2D spectra not shown), are presented in **Fig. S10**. Please refer to **Fig. S11** for atom labelling. Only long-range CH–CH correlations are labelled in **Fig. S9**. Appearance of one-bond correlations in the long-range optimised experiments is possible due to the fast evolution of the $^1J_{CC}$ coupling constant, these correlations were identified by comparison with the $^1J_{CC}$-optimised spectra. The long-range SQ ADEQUATE spectra provide valuable structural information regarding the connectivity of the monosaccharide units within the pentasaccharide, these correlations are labelled in bold.

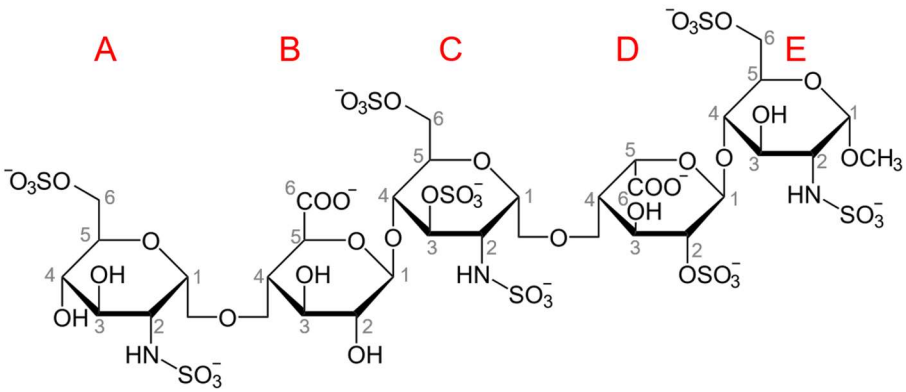

Fig. S11. Labelled structure of fondaparinux (**III**).

Table S3. Signal-to-noise ratio (SNR) comparison for correlations of **III** observed in $^{1}J_{CC}$-optimised SQ ADEQUATE spectra with and without $^{1}J_{CH}$ refocussing.

Correlation (^{1}H, ^{13}C)	Signal-to-noise ratio		**Correlation (^{1}H, ^{13}C)**	Signal-to-noise ratio	
	standard	$^{1}J_{CH}$-refocussed		standard	$^{1}J_{CH}$-refocussed
1A, 2A	8.9	15.5	3C, 4C	2.2[a]	7.8
2A, 1A	4.1	7.5	4C, 3C	4.1	10.7
2A, 3A	3.3	7.2	4C, 5C	2.6[a]	6.3
3A, 2A	3.8	7.5	5C, 4C	– [b]	7.3
3A, 4A	2.3[a]	5.4	1D, 2D	3.4	11.3
4A, 3A	2.0[a]	6.1	2D, 1D	3.1	6.5
4A, 5A	– [b]	4.9	2D, 3D	4.9	7.3
5A, 4A	– [b]	3.6	3D, 2D	2.6[a]	9.2
1B, 2B	2.2[a]	9.6	3D, 4D	3.6	9.0
2B, 1B	3.4	7.2	4D, 3D	10.0[d,e]	25.5[e]
2B, 3B	– [b]	5.9	4D, 5D	10.0[e]	25.5[e]
3B, 2B	2.9[a]	8.4	5D, 4D	6.6	14.5
3B, 4B	– [b,c]	– [b,c]	1E, 2E	6.9	16.0
4B, 3B	– [b,c]	– [b,c]	2E, 1E	4.6	8.3
4B, 5B	3.7[d]	5.2	2E, 3E	3.5	8.5
5B, 4B	– [b,c]	– [b,c]	3E, 2E	3.8	11.2
1C, 2C	4.8	17.3	3E, 4E	2.6[a]	7.3
2C, 1C	3.0[a]	6.5	4E, 3E	3.2	6.6
2C, 3C	2.5[a]	10.0	4E, 5E	3.5	8.4
3C, 2C	2.6[a]	9.4	5E, 4E	– [b]	– [b]

[a] Correlations with SNR ≤ 3 cannot be distinguished from noise without prior knowledge. [b] Not observed. [c] The lack of observable correlation could be explained by strong coupling between protons and/or carbons involved in the coherence. [d] Correlation intensity may be affected by HSQC-like artefact. [e] Overlapping correlations.

Table S4. Signal-to-noise ratio (SNR) comparison for select correlations of **III** observed in $^{n}J_{CC}$-optimised SQ ADEQUATE spectra with and without $^{1}J_{CH}$ refocussing. Correlations between adjacent monomer units are presented in bold as these provide important linkage information.

Correlation (^{1}H, ^{13}C)	Signal-to-noise ratio	
	standard	$^{1}J_{CH}$-refocussed
1A, 5A	– [b]	3.7
1A, 5B	2.7	6.2
1B, 3B	2.9	6.0
2B, 4C	– [b]	3.3
3B, 1B	2.2	5.5
3B, 5B	2.8	5.3
1C, 3D	2.5	4.7
1D, 3D	– [b]	3.2
2D, 4E	2.7	8.2
4D, 2C	– [b]	4.5
5D, 1C	3.1	4.1
5D, 2D	3.1	7.4
2E, 4E	– [b]	5.4

[a] Correlations with SNR ≤ 3 cannot be distinguished from noise without prior knowledge. [b] Not observed.

7. $^{1}J_{CH}$-refocussed DQ ADEQUATE pulse program

```
;adeq11etgpsp.js
;based on adeq11etgpsp
;1,1/1,n-ADEQUATE: 2D-HSQC-1J(CC)/nJ(CC)-ADEQUATE
;                  using sensitivity improvement
;phase sensitive using Echo/Antiecho gradient selection
;with decoupling during acquisition
;using shaped pulses for 180degree pulses on f2 - channel
;with 1JCH refocussing and 1H decoupling for sensitivity improvement
;DQ in F1
;
;J. Sakas & D. Uhrin
;B. Reif, M. Koeck, R. Kerssebaum, H. Kang, W. Fenical & C. Griesinger
;   J. Magn. Reson. A118, 282-285 (1996).
;
;$CLASS=HighRes
;$DIM=2D
;$TYPE=
;$SUBTYPE=
;$COMMENT=


#include <Avance.incl>
#include <Delay.incl>
#include <Grad.incl>


"p2=p1*2"
"p0=p3*4/3"

"d0=3u"
"d11=30m"

"d3=1s/(cnst2*2)-4u"
"d4=1s/(cnst2*4)"
"d23=1s/(cnst3*4)"
"d24=1s/(cnst2*4)"

"in0=inf1/2"

"DELTA1=p16+d16-d0*2+4u"
"DELTA2=p16+d16+8u"
"DELTA3=d23-p24/2-d16-p16-d16-p16-8u"
"DELTA4=d4-p14/2"
"DELTA5=d23-p24/2-4u"
"DELTA6=d4-cnst17*p24/2-4u"
"DELTA7=d23-d3-p24/2-4u"

1 ze
  d11 pl12:f2
2 d11 do:f2
  4u BLKGRAD
  d1 pl2:f2
  (p3 ph1):f2
  4u pl1:f1
  50u UNBLKGRAD
```

```
  p16:gp7
  d16
3 (p1 ph1)
  4u
  DELTA4 pl0:f2
  (center (p2 ph1) (p14:sp3 ph1):f2 )
  4u
  DELTA4 pl2:f2
  (p1 ph2) (p3 ph4):f2
  4u
  d3 pl0:f2 pl19:f1
  DELTA7 cpds1:f1
  (p24:sp7 ph8:r):f2
  4u
  DELTA5 pl2:f2
  (p3 ph9):f2
  d0
  d0
  DELTA1 pl0:f2 do:f1
  (p24:sp7 ph11:r):f2
  4u
  p16:gp1
  d16 pl2:f2
  (p0 ph10):f2
  4u
  p16:gp2
  d16 pl1:f1
  4u
  (p2 ph1):f1
  DELTA2 pl19:f1
  DELTA3 cpds1:f1 pl0:f2
  (p24:sp7 ph11:r):f2
  4u
  DELTA7 pl2:f2
  d3 do:f1
  4u pl1:f1
  (center (p1 ph1) (p3 ph5):f2 )
  4u
  DELTA6 pl0:f2
  (center (p2 ph1) (p24:sp7 ph12:r):f2 )
  4u
  DELTA6 pl2:f2
  (center (p1 ph2) (p3 ph6):f2 )
  4u
  DELTA4 pl0:f2
  (center (p2 ph1) (p14:sp3 ph1):f2 )
  4u
  DELTA4
  (p1 ph1)
  DELTA2
  (p2 ph1)
  4u
  p16:gp3*EA
  d16 pl12:f2
  go=2 ph31 cpd2:f2
  d11 do:f2 mc #0 to 2 F1EA(calgrad(EA) & calph(ph6, +180), caldel(d0,
+in0))
```

```
  4u BLKGRAD
exit


ph1=0
ph2=1
ph4=0 2
ph5=0 0 2 2
ph6=1 1 3 3
ph7=0
ph8=0
ph9=1 1 1 1 3 3 3 3
ph10=1 1 1 1 1 1 1 1 3 3 3 3 3 3 3 3
ph11=1
ph12=0
ph31=3 1 1 3 1 3 3 1 1 3 3 1 3 1 1 3

;pl0 : 0W
;pl1 : f1 channel - power level for pulse (default)
;pl2 : f2 channel - power level for pulse (default)
;pl12: f2 channel - power level for CPD/BB decoupling
;pl19: f1 channel - power level for CPD/BB decoupling
;sp3: f2 channel - shaped pulse (180degree inversion)
;spnam3: Crp60,0.5,20.1
;sp7: f2 channel - shaped pulse (180degree refocussing)
;spnam7: Crp60comp.4
;p0 : f2 channel -  60 degree high power pulse
;p1 : f1 channel -  90 degree high power pulse
;p2 : f1 channel - 180 degree high power pulse
;p3 : f2 channel -  90 degree high power pulse
;p14: f2 channel - 180 degree shaped pulse for inversion
;     = 500usec for Crp60,0.5,20.1
;p16: homospoil/gradient pulse
;p24: f2 channel - 180 degree shaped pulse for refocussing
;     = 2msec for Crp60comp.4
;d0 : incremented delay (2D)                          [3 usec]
;d1 : relaxation delay; 1-5 * T1
;d3 : 1/2J(CH)
;d4 : 1/4J(CH)
;d11: delay for disk I/O                              [30 msec]
;d16: delay for homospoil/gradient recovery
;d23: 1/(4J(CC))
;cnst2 : J(CH) = 127 .. 160 Hz
;cnst3 : J(CC) = 4 .. 8 or 35 .. 55 Hz
;cnst17: = -0.5 for Crp60comp.4
;inf1: 1/SW(DQ-C) = 4 * DW(C)
;in0: 1/(2 * SW(DQ-C)) = 2 * DW(C)
;nd0: 2
;ns: 8 * n
;ds: >= 8
;td1: number of experiments
;FnMODE: echo-antiecho
;cpd1: decoupling according to sequence defined by cpdprg1        [waltz16]
;pcpd1: f1 channel - 90 degree pulse for decoupling sequence      [60 usec]
;cpd2: decoupling according to sequence defined by cpdprg2
;pcpd2: f2 channel - 90 degree pulse for decoupling sequence
```

```
;for z-only gradients:
;gpz1: +78.5%
;gpz2: -77.6%
;gpz3: -59%
;gpz7: -23%

;use gradient files:
;gpnam1: SMSQ10.100
;gpnam2: SMSQ10.100
;gpnam3: SMSQ10.100
;gpnam7: SMSQ10.100
```

8. $^{1}J_{CH}$-refocussed SQ ADEQUATE pulse program

```
;adeq11etgprdsp.js
;based on adeq11etgprdsp
;1,1/1,n-ADEQUATE: 2D-HSQC-1J(CC)/nJ(CC)-ADEQUATE
;   with refocussing of C chemical shift
;   using sensitivity improvement
;phase sensitive using Echo/Antiecho gradient selection
;with decoupling during acquisition
;using shaped pulses for 180degree pulses on f2 - channel
;
;with 1JCH refocussing and 1H decoupling for sensitivity improvement
;SQ in F1
;
;J. Sakas & D. Uhrin
;B. Reif, M. Koeck, R. Kerssebaum, H. Kang, W. Fenical & C. Griesinger
;   J. Magn. Reson. A118, 282-285 (1996).
;M. Koeck, R. Kerssebaum & W. Bermel, Magn. Reson. Chem. 41, 65-69 (2003)
;
;$CLASS=HighRes
;$DIM=2D
;$TYPE=
;$SUBTYPE=
;$COMMENT=


#include <Avance.incl>
#include <Delay.incl>
#include <Grad.incl>


"p2=p1*2"
"p0=p3*4/3"

"d0=3u"
"d11=30m"

"d3=1s/(cnst2*2)"
"d4=1s/(cnst2*4)"
"d23=1s/(cnst3*4)"

"in0=inf1/2"
"in20=in0"
"in21=in0"

"d20=d23-p24/2-d16-p16-d16-p16-p2-8u"
"d21=d23-p24/2-d3-20u"

"td1=tdmax(td1,d20*2,in20)"

"DELTA1=p16+d16+4u-2*d0"
"DELTA2=p16+d16+8u"
"DELTA4=d4-p14/2-4u"
"DELTA5=d23-p24/2-4u"
"DELTA6=d4-cnst17*p24/2-4u"
"DELTA7=d23-p24/2-4u-d3"
```

```
1 ze
  d11 pl12:f2
2 d11 do:f2
  4u BLKGRAD
  d1 pl2:f2
  (p3 ph1):f2
  4u pl1:f1
  50u UNBLKGRAD
  p16:gp7
  d16
3 (p1 ph1)
  4u
  DELTA4 pl0:f2
  (center (p2 ph1) (p14:sp3 ph1):f2 )
  4u
  DELTA4 pl2:f2
  (p1 ph2) (p3 ph4):f2
  4u pl0:f2 pl19:f1
  d3
  DELTA7 cpds1:f1 ph1
  (p24:sp7 ph8):f2
  4u
  DELTA5 pl2:f2
  (p3 ph9):f2
  d0
  d0
  DELTA1 pl0:f2 do:f1
  (p24:sp7 ph11):f2
  4u
  p16:gp1
  d16 pl2:f2
  (p0 ph10):f2
  4u
  p16:gp2
  d16 pl1:f1
  4u
  (p2 ph1):f1
  DELTA2 pl19:f1
  d20 pl0:f2 cpds1:f1
  (p24:sp7 ph11):f2
  d21 pl2:f2
  20u do:f1
  d3 pl1:f1
  (center (p1 ph1) (p3 ph5):f2 )
  4u
  DELTA6 pl0:f2
  (center (p2 ph1) (p24:sp7 ph1):f2 )
  4u
  DELTA6 pl2:f2
  (center (p1 ph2) (p3 ph6):f2 )
  4u
  DELTA4 pl0:f2
  (center (p2 ph1) (p14:sp3 ph1):f2 )
  4u
  DELTA4
  (p1 ph1)
  DELTA2
```

```
  (p2 ph1)
  4u
  p16:gp3*EA
  d16 pl12:f2
  go=2 ph31 cpd2:f2
  d11 do:f2 mc #0 to 2 F1EA(calgrad(EA) & calph(ph6, +180), caldel(d0,
+in0) & caldel(d20, -in20) & caldel(d21, +in21))
  4u BLKGRAD
exit


ph1=0
ph2=1
ph4=0 2
ph5=0 0 2 2
ph6=1 1 3 3
ph7=0
ph8=0
ph9=1 1 1 1 3 3 3 3
ph10=1 1 1 1 1 1 1 1 3 3 3 3 3 3 3 3
ph11=1
ph31=3 1 1 3 1 3 3 1 1 3 3 1 3 1 1 3


;pl0 : 0W
;pl1 : f1 channel - power level for pulse (default)
;pl2 : f2 channel - power level for pulse (default)
;pl12: f2 channel - power level for CPD/BB decoupling
;sp3: f2 channel - shaped pulse (180degree inversion)
;spnam3: Crp60,0.5,20.1
;sp7: f2 channel - shaped pulse (180degree refocussing)
;spnam7: Crp60comp.4
;p0 : f2 channel - 120 degree high power pulse
;p1 : f1 channel -  90 degree high power pulse
;p2 : f1 channel - 180 degree high power pulse
;p3 : f2 channel -  90 degree high power pulse
;p14: f2 channel - 180 degree shaped pulse for inversion
;     = 500usec for Crp60,0.5,20.1
;p16: homospoil/gradient pulse
;p24: f2 channel - 180 degree shaped pulse for refocussing
;     = 2msec for Crp60comp.4
;d0 : incremented delay (2D)                          [3 usec]
;d1 : relaxation delay; 1-5 * T1
;d3 : 1/2J(CH)
;d4 : 1/4J(CH)
;d11: delay for disk I/O                              [30 msec]
;d16: delay for homospoil/gradient recovery
;d20: decremented delay (2D)
;d21: incremented delay (2D)
;d23: 1/(4J(CC))
;cnst2 : J(CH) = 127 .. 160 Hz
;cnst3 : J(CC) = 4 .. 8 or 35 .. 55 Hz
;cnst17: = -0.5 for Crp60comp.4
;inf1: 1/SW(C) = 2 * DW(C)
;in0: 1/(2 * SW(C)) = DW(C)
;nd0: 2
;in20: = in0
```

```
;in21: = in0
;ns: 8 * n
;ds: >= 8
;td1: number of experiments
;FnMODE: echo-antiecho
;cpd1: decoupling according to sequence defined by cpdprg1        [waltz16]
;pcpd1: f1 channel - 90 degree pulse for decoupling sequence      [60 usec]
;cpd2: decoupling according to sequence defined by cpdprg2
;pcpd2: f2 channel - 90 degree pulse for decoupling sequence


;for z-only gradients:
;gpz1: +78.5%
;gpz2: -77.6%
;gpz3: -59%
;gpz7: -23%

;use gradient files:
;gpnam1: SMSQ10.100
;gpnam2: SMSQ10.100
;gpnam3: SMSQ10.100
;gpnam7: SMSQ10.100
```